Preprints of the 19th World Congress
The International Federation of Automatic Control
Cape Town, South Africa. August 24-29, 2014

Adaptive FOCV-based Control Scheme to improve the MPP Tracking Performance: an experimental validation

A. Frezzetti * **S. Manfredi** *,** **A. Suardi** **

* *Automatic Control Group (e-mail: antonio.frezzetti@unina.it, smanfred@unina.it), Department of Electrical Engineering and Technology Information (DIETI), University of Naples "Federico II", IT.*
** *Control and Power Group (e-mail: s.manfredi@imperial.ac.uk) and Circuits and Systems Group (e-mail: a.suardi@imperial.ac.uk), Department of Electrical and Electronic Engineering, Imperial College London, UK.*

Abstract: Nowadays the photovoltaic (PV) is one of the most renewable source device used in the harvesting system to support the life time of stand alone devices like sensor node. One of the most diffused method to increase the PV efficiency is the Fractional Open-Circuit Voltage (FOCV) that allows the PV to work around its estimated Maximum Power Point (MPP). To increase the solar harvesting system efficiency both static (in terms of efficiency) and dynamic (in terms of MPP tracking responsiveness) performances are of crucial interest. Most of works in the literature focus on improving the static system performance by giving a more accurate MPP estimation. In this paper, it is proposed a FOCV-based algorithm to improve system dynamic performance in terms of MPP tracking performance and energy conveyed to the load under varying solar irradiance conditions. The MPP system dynamically adapts the MPP estimation to the solar irradiance condition by mean of a "smart timer" circuitry that continuously adjusts the operative frequency of the sample and hold component. A detailed hardware implementation description of a smart timer as well as a related analytical analysis used for component design are presented. An experimental validation and a comparison of the proposed approach than the standard FOCV based method are carried out. The results show the effectiveness of the proposed scheme in improving dynamic system performance in terms of tracking performance and timeless to convey solar energy to the load storage component (i.e. ultracapacitor).

1. INTRODUCTION

The recent development of low cost smart sensors and microcontrollers supporting network connectivity (Report [2004]) has enabled a fast implementation of distributed consensus and non-consensus based monitoring and control algorithms in many industrial and civilian applications (i.e. military, agriculture, environment monitoring) (Heinzelman [2002], Neumann [2007], Canale [2013], DiGiorgio [2013], Manfredi [2012]). In lack of grid connection, low-power electronics can be partially or completely supplied by renewable power generator. Among different renewable devices, the photovoltaic (PV) source is one of the most used. To face up the variable availability of solar power during each day, the energy can be harvested in a storage buffer (a battery or a ultracapacitor) which is linked to the PV cell by an interposed energy-conditioning block. A control scheme is required to allow the PV source to work at its maximum power operative point. This allows to increase the energy transferred to the storage component (i.e. ultracapacitor) according to the scheme in Fig. 1. Several MPPT control methods have been developed in literature. We can distinguish between inline and offline algorithms. In the former category, the MPPT tunes the polarization point of the PV cell until the maximum power point is reached. Examples of inline algorithms are: Perturb and Observe (P&O) and the Incremental Conductance. Due to the complexity of harvesting system, a relatively powerful microcontroller is typically needed to implement them, which increases the cost of the power consumption. At the opposite, the offline algorithms are based on a less complicated way of tracking the maximum power point. In these methods, the maximum PV voltage V_{mpp} (the maximum current I_{mpp}) is estimated as a function of the PV cell open circuit voltage V_{oc} (Schoeman [1982]) (short circuit current I_{sc}, (Noguchi [2000])). The differences among inline and offline algorithms consist of different levels of precision of the MPP tracking (Zheng [2012]). While in high power applications the ideal MPPT maximizes the tracking efficiency (Manfredi [2012]), in low power applications it is suitable that MPPT power consumption is minimized (Ahmad [2009]).

The Fractional Open Circuit Voltage (FOCV) method (Simjee [2008]) is an offline algorithm typically used for low power applications because it merges good MPPT capability and low power consumption performance. The estimation $\widehat{V}_{mpp}$ of the PV maximum power point voltage, V_{mpp}, depends on the open-circuit voltage V_{oc} by the relation $\widehat{V}_{mpp} = \sigma_v \cdot V_{oc}$ ($\widehat{V}_{mpp} = V_{oc}$ when the PV is

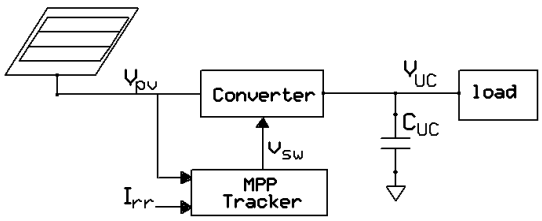

Fig. 1. The proposed MPPT topology.

in the open circuit mode). In the above estimation law, σ_v is characteristic of the PV cell considered and can be experimentally estimated. It has been studied that for each PV cell σ_v is slightly constant for almost any level of irradiation, (Simjee [2008]). With this introduction, the FOCV algorithm periodically samples the Open-Circuit Voltage of the cell, V_{oc}, in order to estimate $\widehat{V}_{mpp}$ by a linear estimation law and, finally, to polarize the PV cell around the estimated $\widehat{V}_{mpp}$. Estimations are periodically repeated with a fixed sampling period of time in order to adapt $\widehat{V}_{mpp}$ to the varying solar irradiance conditions during the day.

Different improvements to the basic FOCV method are proposed in literature. In (Scarpa [2009]) and (Yang [2013]) the authors focus on the static PV characterization. Specifically, they introduce a non linear function of V_{mpp} on the V_{oc} to better evaluate the MPPT estimation, thus improving the static performance in terms of power efficiency. Few works in the literature try to improve dynamic performance of the FOCV-based controller under varying solar irradiance conditions. In (Lapena [2012]) authors propose a low-power FOCV so that the sample and hold of the V_{oc} is adjusted on the base of the solar irradiance by mean of PV current measurement. This paper presents an adaptive low-power MPPT system based on the FOCV method. Similarly to (Lapena [2012]), we implement a controller that adaptively changes its tracking accuracy as function of the solar irradiance. Differently than the approach in (Lapena [2012]), we propose an alternative hardware MPPT implementation that continuously adapts the MPP estimation frequency to the varying solar irradiance. Additionally the evaluation of the different irradiance condition is carried out by mean of a photoresistor in place of the PV current sensor. In this way, the controller has a transduced measurement directly related to the level of solar energy, differently than the PV current sensor that indirectly depends on the solar irradiance. Indeed the latter measurement may lead with irradiance evaluations that can be affected by parametric variations, temperature fluctuations or health conditions of the PV cell. Moreover, an analytical analysis of the proposed scheme and an identification of σ_v parameter procedure are presented. These may help the designer in tuning the system parameters.

The paper is organized as follows. In Sec. 2, we give the block description of the proposed adaptive MPPT. Then we illustrate an identification procedure to estimate the value of σ_v of a PV cell. Then, in Sec. 3 the adaptive FOCV control scheme based on a smart timer is presented. Details about the smart timer analysis as well as its hardware implementation are given. Finally, in Sec. 4 an experimental validation of the proposed scheme and its comparison than the standard FOCV standard scheme are presented

2. THE PROPOSED ADAPTIVE FOCV SCHEME

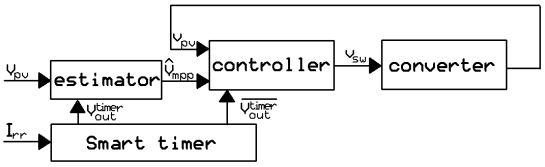

Fig. 2. Block diagram of the MPPT scheme.

In Fig. 2 the block diagram of the proposed FOCV control is depicted. The estimator block provides the evaluation of $\widehat{V}_{mpp}$ by the formula $\widehat{V}_{mpp} = \sigma_v \cdot V_{oc}$. During the harvesting period, the controller block senses the V_{pv} voltage and polarizes the cell to get $V_{pv} \sim \widehat{V}_{mpp}$. In the following, T_H and T_L respectively refer to the time duration of estimation and harvesting phases. Both estimator and controller blocks are enabled or disabled by mean of V_{OUT}^{timer} that is generated by the Smart timer block (described later in details). During the estimation time T_H, the controller is disabled while the estimator block is enabled. During this period of time, V_{pv} reaches the open-circuit voltage V_{oc} and the estimator block evaluates $\widehat{V}_{mpp}$ with $\widehat{V}_{mpp} = \sigma_v \cdot V_{oc}$. On the opposite, during the harvesting period of time T_L, the estimator block is disabled and the controller is able to polarize the PV cell at $\widehat{V}_{mpp}$ voltage. Therefore:

$$V_{OUT}^{timer} = \begin{cases} 1 & \text{during the estimation time, } T_H \\ 0 & \text{during the harvesting time, } T_L \end{cases}$$

Typically, T_H is lower than T_L because the MPPT spends the most of time for the energy harvesting process. Therefore, we can assume that $T_H < T_L$. The enhancement we have introduced is on the adaptation of the harvesting time T_L by a smart timer that adjusts the sample time of the V_{oc}. The Smart timer adaptively varies T_L on the base of the variation of solar irradiance conditions, I_{rr}. In the following of this section, we will describe the estimator and the controller blocks in Fig. 2.

2.1 FOCV-based adaptive estimator

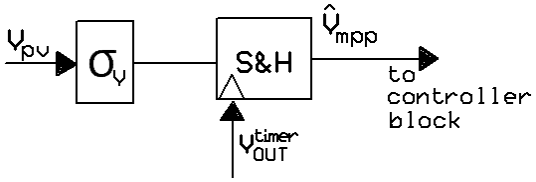

Fig. 3. Estimator block scheme.

In Fig. 3 the scheme that implements the estimation $\widehat{V}_{mpp} = \sigma_v \cdot V_{oc}$ is presented, where $\widehat{V}_{mpp}$ is defined as:

$$\widehat{V}_{mpp}(k) = \begin{cases} \sigma_v \cdot V_{oc}(k) & \text{if } V_{OUT}^{timer} = 1 \\ \widehat{V}_{mpp}(k-1) & \text{if } V_{OUT}^{timer} = 0 \end{cases} \quad (1)$$

for each $k \in \mathbb{N}$, being k the discrete sample time and V_{OUT}^{timer} the output of the Smart Timer block in Fig. 2. The value of σ_v in (1) depends on the employed PV cell. We implement

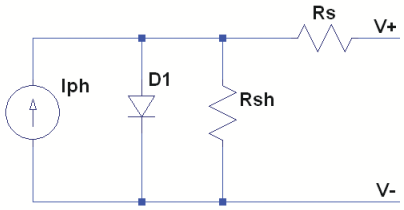

Fig. 4. Xiao model with the addiction of R_{sh} as a term of loss.

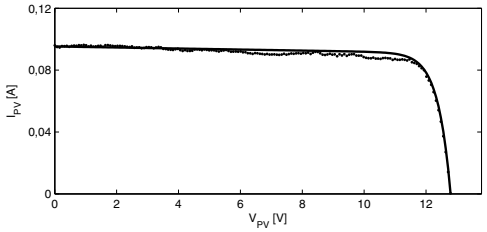

Fig. 5. PV source Voltage-Current identification: experimental curve (dotted line) and modified Xiao's model (continuous line) curve.

an identification procedure by Xiao in (Xiao [2004]) in order to identify the model parameters of the photovoltaic device. Then, we use this PV model to calculate the σ_v value. We have considered the PV model depicted in Fig. 4, that is the Xiao's model with a loss resistance R_{sh}. It is a classical single-diode model and includes four components: a (photo)current source I_{ph}, a diode $D1$ in parallel to the source, series R_s and shunt R_{sh} resistors. The model parameters have been identified in order to fit the theoretical curve with the experimental one (derived by the available data). The result of the identification is depicted in Fig. 5, while the numerical value of parameters and their meanings are both summarized in Table 1. Once the adopted PV model is found, we can calculate the V_{mpp} from the model and finally, we can obtain σ_v by the relation $\sigma_v = \frac{V_{mpp}}{V_{oc}}$. In our case, the identification procedure yields to $\sigma_v = 0.76$. Notice that experimental results show that the value of σ_v is almost constant for any irradiance conditions (Simjee [2008]).

2.2 Controller

The controller manages the PV operating point to stay close the estimated maximum power point. It is a switching ON/OFF controller with an hysteresis V_H. In Fig. 6, $Cont_{Hyst}$ is an hysteresis comparator that generates the control signal V_{SW} for the converter (Fig. 1). Control is based on the comparison between the instantaneous voltage of the cell, V_{pv}, and $\widehat{V}_{mpp}$ according to the law:

$$V_{SW}(t) = \begin{cases} V_{low} & \text{if } V_{pv}(t) - \widehat{V}_{mpp} \leq -V_H \text{ and } V_{OUT}^{timer} = 0 \\ V_{high} & \text{if } V_{pv}(t) - \widehat{V}_{mpp} \geq V_H \text{ and } V_{OUT}^{timer} = 0 \\ V_{low} & V_{OUT}^{timer} = 1 \end{cases} \quad (2)$$

where V_{low} and V_{high} respectively denote the low and high values of V_{SW}. Specifically, the behavior of the controller can be summarized as follows: when $V_{SW} = V_{high}$, energy is harvested, $V_{pv}(t)$ decreases until V_{SW} switches to V_{low}.

Model parameters	Value	Meaning
T_j	290 K	Junction temperature
n	15.5	diode un-ideal factor
V_{oc}	12.55V	PV open circuit voltage
i_{pv}	0.995A	PV short circuit voltage
I_s	1.2fA	diode saturation current
R_s	0.761 $\rho\Omega$	series resistance
R_{sh}	12.5 kΩ	Pv open circuit voltage

Table 1. Xiao's model parameters

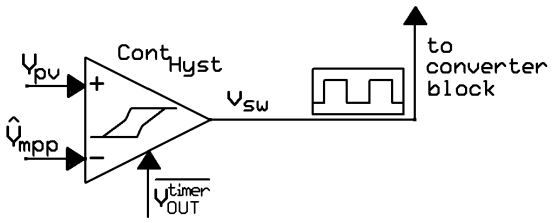

Fig. 6. Block diagram of the proposed controller.

Consequently, the harvesting process is inhibited, $V_{pv}(t)$ increases and this condition holds until $V_{pv}(t) = V_{high}$. Then, another cycle restarts. In conclusion, the PV cell with the control law given in (2) works at its expected MPP. As depicted in Fig. 6, the controller is enabled by the output signal of the smart timer. The controller is implemented by a standard circuit comparator shown in Fig. 6. In the following we will detail the smart timer hardware implementation, its analysis and design.

3. THE ADAPTIVE SMART TIMER: ANALYSIS, DESIGN AND IMPLEMENTATION

Let δ_{st} be the duty cycle of the squared signal V_{OUT}^{timer}

$$\delta_{st} = \frac{T_L}{T_H + T_L}$$

we note that high value of δ_{st} corresponds to spend more time in harvesting phase (i.e. $T_H \ll T_L$), while low values implies that the $\widehat{V}_{mpp}$ is carried out more frequently. By at large, there is a trade off between the amount of energy harvested and the tracking performance of the variable maximum power point. In other words, the selection of the δ_{st} value impacts on the overall performance. In this paper, we propose to adapt δ_{st} as function of the solar irradiance I_{rr}. The required behavior of the proposed adaptive scheme is:

(a) at low irradiance conditions, a low estimation frequency is required in order to reduce the dynamic power loss related to the estimation process. Moreover, at this low efficiency operative point (low irradiance condition), the system should spend more time in the harvesting phase, trying to transfer to the storage device energy as soon as possible. On the other hand, at higher value of irradiance condition, it is required an increase of the MPP estimation frequency so that the system spends relatively more time in the estimation phase improving its tracking MPPT performance, thus pulling out more energy from the solar panel. Additionally, this increases the system responsiveness under varying solar irradiance conditions and improves the dynamic performance of the Ultracapacitor charging phase.

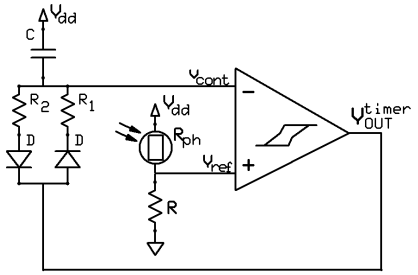

Fig. 7. Physical implementation of the proposed Smart timer.

Behavior *(a)* implies that δ_{st} is inversely proportional to I_{rr}. The proposed smart timer implementation is shown in Fig. 7. In the following, we will carry out an analytical derivation of T_H and T_L.

Let define with V_{ref} the reference signal and with $v_{cont}(t)$ the control signal of the proposed timer. Let define t_0 : $V_{OUT}^{timer}(t_0) = 1$ and t_1 : $V_{OUT}^{timer}(t_1) = 0$, according to the scheme, the dynamic of v_{cont} is described by:

$$v_{cont}(t) = V_{dd} \cdot (1 - e^{-\frac{t}{\tau_1}}) \tag{3}$$

with $\tau_1 = R_1 \cdot C$ and V_{dd} the drain voltage of the circuitry, stated the following initial and final condition:

$$\begin{aligned} v_{cont}(t_0) &= V_{ref} - \frac{\Delta V_{Hyst}}{2} \\ v_{cont}(t_0 + T_H) &= V_{ref} + \frac{\Delta V_{Hyst}}{2} \end{aligned} \tag{4}$$

By (3) and (4), it can be easily derived that:

$$T_H = \tau_1 \cdot ln\left(1 + \frac{2 \cdot \Delta V_{Hyst}}{2V_{dd} - 2V_{ref} - \Delta V_{Hyst}}\right) \tag{5}$$

On the opposite, when $V_{OUT}^{timer}(t_1) = 0$ the control voltage $v_{cont}(t)$ satisfies the condition: $v_{cont}(t_1) = V_{ref} + \frac{\Delta V_{Hyst}}{2}$. During time $t > t_1$ the voltage $v_{cont}(t)$ is driven low by V_{OUT}^{timer} by an exponential law given by: $v_{cont}(t) = (V_{ref} + \frac{\Delta V_{Hyst}}{2}) \cdot e^{-\frac{t-t_1}{\tau_2}}$, being $\tau_2 = R_2 \cdot C$. After T_L, the condition $v_{cont}(t_1 + T_L) = V_{ref} - \frac{\Delta V_{Hyst}}{2}$ holds and V_{OUT}^{timer} switches to his high state. The same derivation given above yields to:

$$T_L = \tau_2 \cdot ln\left(1 + \frac{2 \cdot \Delta V_{Hyst}}{2V_{ref} - \Delta V_{Hyst}}\right) \tag{6}$$

By (5) and (6) it appears that T_H and T_L can be designed as function of V_{ref}, τ_1, τ_2 and ΔV_{Hyst}. For instance, for a given value of T_L, we can design T_H so that $T_H < T_L$ if we choose a time constant τ_1 lower than τ_2. In order to adapt δ_{st} as function of the irradiance I_{rr}, we introduce a photoresistor R_{ph} in a voltage divider configuration along with the resistor R. Among different kind of photoresistors, we choose one with negative characteristic (i.e. the value of resistance R_{ph} reduces when the irradiance I_{rr} increases) so that V_{ref} increases for increasing value of irradiance condition according to:

$$V_{ref} = \frac{R}{R_{ph}(I_{rr}) + R} V_{dd} \tag{7}$$

If we choose $R_{ph} \gg R$ (i.e. $R_{ph} \sim M\Omega$ and $R \sim k\Omega$) then it results $V_{ref} \sim \frac{R}{R_{ph}(I_{rr})} V_{dd}$ (i.e. $V_{ref} \ll V_{dd}$). From (5) if $V_{ref} \ll V_{dd}$, then T_H becomes approximately constant with I_{rr}. Moreover, taking into account (5), (6) and (7) it follows:

$$\begin{cases} T_H \sim \tau_1 \cdot ln\left(1 + \dfrac{\Delta V_{Hyst}}{V_{dd}}\right) \\ T_L(I_{rr}) = \tau_2 \cdot ln\left(1 + \dfrac{2 \cdot \Delta V_{Hyst}}{2\left(\frac{R}{R_{ph}(I_{rr})} V_{dd}\right) - \Delta V_{Hyst}}\right) \end{cases} \tag{8}$$

In (8) we have used the approximation $\Delta V_{Hyst} < V_{ref} \ll V_{dd}$. By using a photoresistor with negative characteristic it results that T_L decreases when I_{rr} increases and, finally, we have that δ_{st} is inversely proportional to the irradiance level I_{rr} according to:

$$\delta_{st} = \frac{1}{1 + \frac{T_H}{T_L(R_{ph}(I_{rr}))}} \tag{9}$$

Component ID and function	*Application*
LTC1440 Hysteresis voltage amplifier	Estimator: V_{oc} voltage sensing block Controller: hysteresis comparator block Smart timer: hysteresis comparator block
DG412 Sample and Hold	Estimator: V_{oc} Sample and Hold block
NSL-19M51 photoresistor	Smart timer: negative photoresistor

Table 2. Components of the hardware implementation of Sec. 4.

4. EXPERIMENTAL VALIDATION

In this section, we show the effectiveness of the adaptive FOCV-based method. The proposed MPPT scheme has been experimentally implemented and indoor tests have been carried out. The main hardware components adopted into our prototype are summarized in Table 2. During indoor tests, a lamp with tunable brightness emulates the solar irradiance variation over time.

Firstly, we verified that the proposed Smart timer behaves as postulated above. Fig. 8(a) shows the experimental evolution for δ_{st} under increasing lamp brightness, confirming the expected theoretical behavior in (9).

To experimentally validate the effectiveness of the proposed adaptive scheme, we propose to compare one complete UC charging cycle when the adaptive FOCV and the standard (non adaptive) FOCV approach are implemented. In Fig. 8(b) the experimental results are shown: the continuous line represents the charging curve when the adaptive FOCV-based MPPT controller is adopted, while the dashed line is the experiment result for the standard FOCV method case. Notice that the experiments have been carried out starting from the same initial conditions and under the same environmental scenario (i.e. same brightness variations). Fig. 8(b) clearly shows the effectiveness of the proposed scheme because it speeds up the ultracapacitor recharging process, increasing the dynamic efficiency of the overall system.

5. CONCLUSION

In this paper we presented an adaptive FOCV-based controller to deal with solar irradiance environment variations. The implementation scheme has been described and

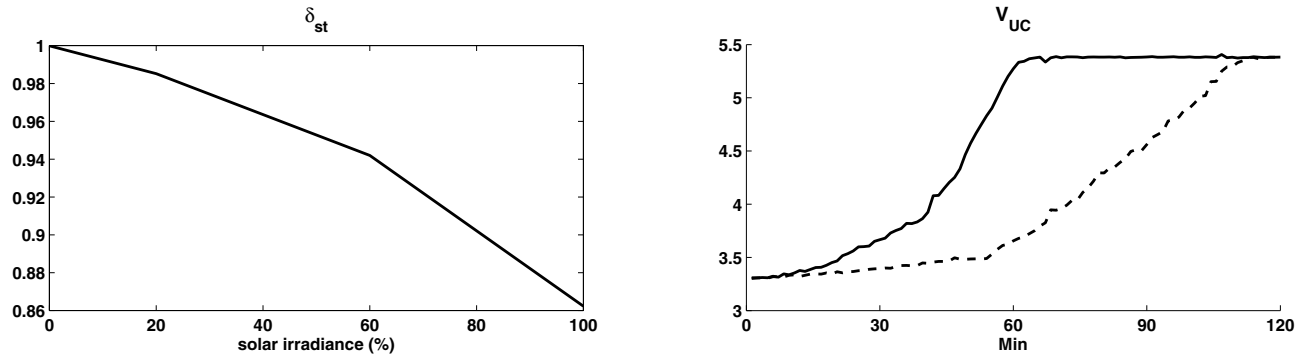

Fig. 8. Experimental validation: **(a)**: measured δ_{st}; **(b)** V_{UC} ultracapacitor voltage for the proposed adaptive scheme (continuous line) and standard scheme (dashed line).

the details of the design have been presented. Finally, we demonstrate the effectiveness of our controller by experimentally comparing performance of the proposed adaptive MPPT with classical FOCV method. The results show that the proposed scheme is effective in improving the dynamic performance of the overall harvesting system.

REFERENCES

Report. *Industrial Wireless Technology for the 21st Century.* Technology Foresight, 2004, TF-2004-1.

W. Heinzelman, A. Chandrakasan and H. Balakrishnan. *An Application-Specific Algorithm Architecture for Wireless Microsensor Networks.* IEEE Transactions on Wireless Communications, 2002.

P. Neumann. *Communication in industrial automation-What is going on?.* Control Engineering Practice, Volume 15, Issue 11, November 2007.

S. Canale, A. Di Giorgio, A. Lanna, A. Mercurio, M. Panfili, A. Pietrabissa, *Optimal planning and routing in Medium Voltage PowerLine Communications networks* IEEE Transactions on Smart Grid (IEEE Control System Society, USA), Vol. 4, Issue: 2, June 2013, pp. 711-719, DOI: 10.1109/TSG.2012.2212469.

A. Di Giorgio, F. Liberati, A. Pietrabissa, *On-board stochastic control of Electric Vehicle recharging* 52nd IEEE Conference on Decision and Control (CDC 2013), December 10-13, 2013, Florence, Italy.

S. Manfredi, *A consensus based rate control scheme for ATM networks* International Journal of Control, Automation and Systems, 10 (4), pp. 817-823. doi: 10.1007/s12555-012-0418-1.

J. J. Schoeman and J. D. VanWyk, *A simplified maximal power controller for terrestrial photovoltaic panel arrays.* In Proceedings 13th Annual IEEE Power Electronics, 1982.

T. Noguchi, S. Togashi, and R. Nakamoto. *Short-current pulse based adaptive maximum-power-point tracking for photovoltaic power generation system.* In Proceedings IEEE International Symposium Industrial Electronics, 2000.

H. Zheng, S. Li. *Comparative Study of Maximum Power Point Tracking Control Strategies for Solar PV Systems.* Transmission and Distribution Conference and Exposition, 2012.

S. Manfredi, M. Pagano, R. Raimo. *Ultracapacitor-based distributed energy resources to support time-varying smart-grid power flows* SPEEDAM 2012 - 21st International Symposium on Power Electronics, Electrical Drives, Automation and Motion, pp. 1148-1153, ISBN: 978-146731299-8 doi: 10.1109/SPEEDAM.2012.6264610

J. Ahmad and H. Kim. *A Voltage Based Maximum Power Point Tracker for Low Power and Low Cost Photovoltaic Applications.* World Academy of Science, Engineering and Technology, No.60, 2009.

V. Scarpa, S. Buso, and G. Spiazzi. *Low-Complexity MPPT Technique Exploiting the PV Module MPP Locus Characterization.* IEEE Transaction on Industial Electronics, Vol. 56, No. 5, May 2009

Y. Yang, and Z. Yan *A MPPT Method using Piecewise Linear Approximation and Temperature Compensation.* Journal of Computational Information Systems 9: 21 (2013) 86398647.

O. Lopez-Lapena and M.T. Penella, *Low-power FOCV MPPT controller with automatic adjustment of the sample&hold.* Electronics Letters, Vol. 48, No. 20, 2012.

W. Xiao, W. G. Dunford and A. Capel, *A Novel Modeling Method for Photovoltaic Cells.* 35th Annual IEEE Power Electronics Specialists Conference, Aachen, Germany, 2004.

F. I. Simjee and P. H. Chou, *Efficient Charging of Supercapacitors for Extended Lifetime of Wireless Sensor Nodes.* IEEE Transactions on Power Electronics, Vol. 23, 2008